University of Exeter coursework header sheet

ECM3102 Individual Project (Meng) (A, TRM1+2 2015/6)

020822

1019474

620009941

Coursework: Final Report

Submission Deadline: Thu 28th Apr 2016 12:00

Personal tutor: Dr Krisztian Kohary

Marker name: G Tab

Word count: 14242

By submitting coursework you declare that you understand and consent to the University policies regarding plagiarism and mitigation (these can be seen online at www.exeter.ac.uk/plagiarism, and www.exeter.ac.uk/mitigation respectively), and that you have read your school's rules for submission of written coursework, for example rules on maximum and minimum number of words. Indicative/first marks are provisional only.

Final Report

A Modern Benchmark for Automotive Aerodynamic Performance Modelling

Rhys Gilbert

2016

3rd Year Individual Project

I certify that all material in this thesis that is not my own work has been identified and that no material has been included for which a degree has previously been conferred on me.

Signed 

College of Engineering, Mathematics, and Physical Sciences
University of Exeter

Final Report

ECM3101/ECM3102/ECM3149

Title: A Modern Benchmark for Automotive Aerodynamic Performance Modelling
Word count: 14242
Number of pages: 35

Date of submission: Monday, 25 April 2016

Student Name: Rhys Gilbert
Programme: Mechanical Engineering MEng
Student number: 620009941
Candidate number: 020822

Supervisor: Dr Gavin Tabor

Abstract

Computational Fluid Dynamics (CFD) is an area of engineering combining mathematics, physics and computer science. CFD solves the Navier-Stokes equations, which fully describe the motion of a fluid, using computers. CFD solvers require validation against experimental data in order to ensure that the correct flow field is being solved for. It is here where this project comes in, which is to validate CFD codes for the automotive industry along with generating interest and awareness in automotive validation and test cases.

CFD validation cases in the automotive industry are lacking industrially relevant details. The introduction of the DrivAer model by the Technical University of Munich (TUM) hopes to change this. This case introduces a range of industrial geometries with associated experimental data.

Three automotive geometries along with three CFD codes have been chosen to use in this validation, zCFD from Zenotech, Fluent from Ansys and OpenFOAM which is a registered trademark of OpenCFD Limited. In order to undertake CFD validation a few steps are needed to be undertaken. This involves CAD clean-up, meshing of the geometry, solving the Navier-Stokes equations and finally, post processing.

The results show very good agreement, with the largest error being around 3% of the experimental value of the drag coefficient, for both zCFD and Fluent for all three cases investigated. OpenFOAM, on the other hand, has the largest error of 50% from the experimental values of the drag coefficient, and was incapable of running on the most detailed case.

As the aims are to increase awareness of industrially relevant automotive test cases for CFD validation, these results will be presented to industry at an event created by CFMS on the 10th May 2016. Along with this, the results are being submitted for publication at the International Conference of Vehicular Aerodynamics hosted by the Institute of Mechanical Engineers in September 2016. With this there will also be a presentation, if accepted, about the work at this conference.

Keywords: CFD, DrivAer, Automotive, Validation, Fluid Dynamics, Computational Fluid Dynamics

Table of contents

1. Introduction and background

Computational Fluid Dynamics (CFD) has been around since the 1930s. Originally the main focus was on solving two dimensional flows around aerofoil geometry. Since then there have been great advancements in the field. Fully turbulent three dimensional flows are now able to be solved using CFD. These advancements have been due to the increased understanding in fluid flow along with the progression in computing technology. As CFD was mainly developed by the aerospace industry the automotive sector has only recently started using CFD for design and currently lacks the validation and development the aerospace industry has had.

CFD is solely computational, which means that no physical models need be produced, reducing cost and time. As this is of great benefit CFD has been used largely for design. CFD has also been used to advance our understanding of fluid flow. CFD can also be inaccurate as the solution will only be as good as the input files that are given. Therefore it must be used with great caution.

As CFD can be inaccurate, validation of the codes must be undertaken to ensure that the codes can compute accurate results for given problems. This validation is usually undertaken by comparison of CFD data with experimental data. There have been many validation test cases in a variety of areas; however there have been few in the automotive sector.

Unlike the aerospace industry, validation cases for the automotive industry do not come around that often. It is assumed that because the codes are validated for a variety of other cases that they will suffice for the automotive industry. This however may not be the case as some of the modelling in automotive cases may not be validated by aerospace test cases. Along with this there are outdated automotive test cases, which do not necessarily represent the geometries of today's vehicles.

The objectives of this project are to validate a range of CFD codes available, both commercial and open source, against a new industrially relevant case. This will hopefully raise awareness of the limitations of CFD codes on industrially relevant geometries. As a by-product of this investigation a large database full of geometries, experimental results and simulation data will be available for others to use and validate their codes against.

Assumptions made during the course of the project are that the geometries supplied are identical to those tested during the experiment and also that the initial conditions that have been specified are also identical to the wind tunnel data.

The following section will contain a literature review, where previous work conducted about this geometry will be examined and reviewed, along with other related materials.

Following on from this there will be a section on the method of CFD. This will discuss the main method of generating a solution from the geometry stage, from CAD to meshing to solution and post processing. Along with this will be the theory used to generate the solution, including the Navier-Stokes equations, a discussion on turbulence modelling and the description of the turbulence model used, along with the equations used in the post processing of CFD data.

Following this there will be a section on experimental work. This will include an introduction to the solvers used and initial conditions of the case. Also included within this section will be a discussion on the various geometries investigated and why they have industrial relevance and how they stress the turbulence models.

Presentation of the results will follow, which will present the results obtained from the solvers for each of the cases. Following this there will be a discussion on the results, where the results will be described and where conclusions about the flow are drawn. Included in this section will be a conclusion along with what is proposed for further work following this project's conclusion.

Finally there will be a section on project management where all safety and environmental considerations will be discussed.

2. Literature review

Issues arising from automotive sectors of engineering are that the companies avoid publishing data about their geometries as they are in competition with other companies in the same area. This has therefore been a hindrance to the advancement of automotive CFD. NASA has launched the industrially relevant drag prediction workshop to advance CFD for aerospace to validate CFD codes against. However in the automotive industry there have been few proposed test cases.

Initial investigations into automotive geometries were initially investigated in 1984 (Ahmed and Ramm, 1984). This geometry, known as the Ahmed body, has been widely investigated (Linehart *et al*. 2000; Linehart and Becker, 2003; Krajonovic and Davidson, 2004) and has been used as an automotive validation test case for many years.

One benefit of this model is that the rear end of the body has different configurations. Those configurations each have their own experimental data for validation. This geometry has been simulated using new developments in high-order numerical methods (Minguez *et al.* 2008).

Other benefits and a possible reason why the geometry has become a main validation test case is that the geometry is relatively simple. Therefore, with simplified geometry, solution generation becomes less time consuming and results can be validated in less time.

Drawbacks of this geometry are that being a simplified representation of industrial geometry, it does not fully show all the flow characteristics of modern geometry. An example would be that as the underside of the geometry is smooth it does not allow for detailed underbody flow simulations, for example geometry with an exhaust.

Another drawback is that although the geometry has wheel representations these cannot be rotated. As these cannot be rotated this aspect of the modelling cannot be stressed. This, then, does not represent the flow conditions that are being generated by industrially relevant automotive geometries.

One other automotive geometry that has been produced is the SAE body (Wordley and Saunders, 2006; Wordley *et al.* 2007). This geometry is more detailed as it contains open wheel configuration, which is not relevant for industry as the majority of car manufacturers

use closed configurations. This reason is one factor why this test case has not been developed and investigated in as much detail as the Ahmed body.

Benefits of the SAE body include there being experimental data to compare and validate CFD codes against, along with there being an increased relevance to the motor racing area of automotive engineering.

To progress CFD in the automotive industry there has been an industrially relevant case proposed by the Technical University of Munich (TUM). What has been proposed is a series of geometry configurations relevant for industry. There has been collaboration between TUM, Audi and BMW to develop an industrially relevant test case. This test case has been called the DrivAer model and was introduced in 2011.

Initial investigations into the geometry along with experimental data have been introduced and conducted (Heft *et al*. 2011; Thiessen *et al.* 2011; Wojciak *et al*. 2011; Heft *et al*. 2012 (a); Heft *et al.* 2012 (b)) by TUM. Other investigations have been conducted (Guilmineau, 2014; Yazdani, 2015, Ashton *et al.* 2016) into the DrivAer model based on various numerical methods. This test case has already seen a large interest.

One major benefit to the geometry is that it has complete modularity. The geometry includes one main body with three different back end configurations. There are also three underbody configurations, those being smooth underbody with no wheels, smooth underbody with wheels and the fully detailed underbody. As with the underbody there are three different configurations for the wheels, one with smooth surface without alloys, a smooth surface with alloys and a fully detailed surface with alloys. Additional detail can be added in the form of wing mirrors and exhaust pipe.

With the geometry being completely modular it enables quick initial validation of the basic geometry through to the validation of the fully detailed industrially relevant case. Along with this the validation for rotating geometry can be investigated as the wheels are able to be rotated, which increases modelling difficulty.

There are however drawbacks with this geometry. Where a more detailed geometry is investigated, increased time and effort to generate good quality meshes is a consequence leading to the decreased likelihood of companies undertaking the work.

There have already been investigations into this geometry which do not impact onto the work proposed for this investigation. This is due to the objectives of this report being to produce a database of results that can be used in comparison. They also do not impact as the purpose of this work is to raise awareness of this industrially relevant test case and attempt for this to become the standard validation case for the automotive industry.

Having conducted a literature review it is clear that there is a specific need for there to be an automotive industrially relevant test case driven by the lack of current geometries and also the lack of detail on currently used validation cases. One reason for this is that CFD has been adopted early on by the aerospace industry where large strides in validation have taken place whereas the automotive industry has lagged behind.

3. Methodology and theory

In order to complete a CFD validation a few steps need to be undertaken. The initial is geometry generation, which involves drawing the geometry in a computer aided design (CAD) package. From this generation CAD clean-up is undertaken, which produces a watertight surface model. Following this meshing can be carried out, which involves discretising the surface and volume into a finite number of cells. Once the mesh has been produced the solution phase can be undertaken, which involves solving the equations for fluid flow in each of the cells. Post-processing follows and is the generation of usable images and data from the solver phase that can be used in design decision and code validation.

This is the general overview of the process; these steps will be discussed more deeply in the following sections.

3.1. Geometry generation

Geometry generation is of vital importance to the overall accuracy of a CFD simulation. For example, if the underlying geometry is not similar to that being tested in the wind tunnel then even the best, most accurate solvers would not be able to accurately capture the same flow field and generate solutions that are produced by the wind tunnel. Therefore it is of paramount importance that this stage is as accurate as possible to the geometry tested experimentally. This process was not undertaken in this project as the geometry was already provided; it has been included for completeness. It is also assumed that the geometries provided are as accurate and detailed as the geometry used in the wind tunnel experiment.

3.2. CAD clean-up

CAD clean-up is also vitally important for an accurate CFD solution. As the CAD file exported can be in a variety of formats the surfaces exported may not necessarily be connected, which leaves small gaps. For the next stage of the process the surfaces must be completely closed and having no gaps.

This process can be time consuming as to process a detailed case with large number of surfaces can take a while. The importance of this stage is large, as by connecting the surfaces together to remove gaps the underlying geometry may be altered; it is therefore important that again the experimental geometry is adhered to as best as possible.

One other use for CAD clean-up is merging surfaces together. The idea is to merge two or more surfaces that are not connected at a hard edge or where detail may be lost. This reduces the overall number of surfaces and speeds up the next stage. The aim in this stage is to generate a watertight surface model.

3.3. Meshing

Meshing is the process used for discretising a surface or volume up into finite volumes or cells. These are then used in the solver for solving the equations of fluid flow. There are various algorithms for generating these meshes, such as Delaunay triangulation as described in (Lee and Schachter, 1980) or another being the Advancing Front method as described in

(Owen *et al.* 1999). These methods are used for the surface discretisation. Volume meshing follows similar methods.

One issue arising from discretisation is accuracy and how well represented the underlying geometry is. If the surface is adequately discretised and represented then there is a good chance that physical flow phenomena, such as vortices and shear layers, are being modelled. However if the surface is inadequately discretised then the geometry simulated would be different from that of the experiment and the results would be inaccurate.

Another impact is the fineness and coarseness of the mesh. If the mesh is fine, i.e. has small cell sizes, then the regions where there are high gradients of flow and geometrical change would be captured. One drawback from this is that where there are small or zero flow gradients fine cells become inefficient as fewer cells could capture the flow in that region, which leads to an increased solution time.

The opposite could be said in that the coarser the mesh, i.e. has large cells, areas where there is little to no flow gradient would be solved efficiently, whereas regions where there are high solution gradients or geometrical features would not be captured accurately. Therefore there is a balance between fine meshes in regions of high solution gradient and geometrical detail and coarse meshes where there would not be.

There are some criteria that must be considered while creating meshes to give good solution quality. Some include skewness, orthogonality, area or volume ratios, amongst others.

Skewness

Skewness is the measure of how close the cell or face is to the ideal. An example of an ideal face is an equilateral triangle. Skewness is then measured on a scale from 0 to 1. A value of 0 represents that the face is ideal; whereas a value of 1 represents that the face is degenerate or sliver in shape. These values can be controlled by smoothers and refinement while meshing to avoid high skewness areas. A maximum value of 0.9 is recommended to achieve good results. Some solvers fail to run on high skewness meshes, which is why skewness should be kept to a minimum.

$$Skewness = max\left[\frac{\theta_{max} - \theta_e}{180 - \theta_e}, \frac{\theta_e - \theta_{min}}{\theta_e}\right]$$

Equation 1: Where θ_{max} and θ_{min} are the maximum and minimum angles and θ_e is the equi-angular face or cell value.

Orthogonality

Orthogonality criterion is a measure of how the vector from the centroid to its neighbour centroid is in comparison to the face normal vector. Again, as with skewness, this criterion is measured on a scale of 0 to 1 with 0 representing that the vectors are perpendicular and 1 representing parallel. A high value of orthogonality is required, this is due to the solution being solved through the face and added to the values stored at the cell centres. If the face normal does not point in the same direction as the cell centroid vector then the solution being added to the value stored at the cell centre may not represent the actual flow through the centre.

$$Orthogonality = \frac{\boldsymbol{A} \cdot \boldsymbol{f}}{|\boldsymbol{A}||\boldsymbol{f}|}$$

Equation 2: Where **A** is the face normal vector and **f** is the vector between cell centres.

Area or volume ratio

This is a measure of how the volumes compare to those of their neighbours. Ideally there should be a volume ratio of around 100 between cells. This is due to there being a smooth gradient from fine to coarse cells.

yPlus

The yPlus value is associated with wall boundaries. The yPlus value is related to the non-dimensional wall boundary layer profile. This also relates to the first cell height of the mesh, and calculates how high the cell centre is from the wall. In order to calculate the yPlus value for the mesh the following equations are used.

$$y^+ = \frac{\sqrt{\frac{\tau_w}{\rho}}y}{\nu} \qquad \tau_w = \mu\left(\frac{\partial u}{\partial x}\right)_{y=0}$$

Equation 3: Where y^+ is the yPlus value, y is the first cell height, τ_w is the wall shear stress, ρ is the fluid density, ν and μ are the kinematic and dynamic viscosities respectively and u is the velocity parallel to the wall. (Davidson, 2015)

This value which is specified during mesh creation is also dependent on which turbulence model is used, which is discussed in section 3.4.

Mesh independence

In order for the solution from any simulation to be considered reliable there must be a mesh independence study completed. The main reason for this is that the mesh can impact the solution. For example, if there are large cells, these cells could be unable to capture high gradient flow or even separation at the correct point. Therefore by investigating the same case with a variety of different cell sizes, which fundamentally leads to different total number of cells in the meshes, it can be found where the mesh cell size no longer impacts the results of the solution. When this is the case, the solution is deemed mesh independent.

3.4. Solver

All CFD solvers solve the same equations for fluid flow, those equations being the Navier-Stokes equations. These equations are capable of fully representing all flows for all fluids; some modifications are needed for modelling combustion/reacting flows and multiphase flows.

Navier-Stokes

The general Navier-Stokes equations below are in full compressible formulation in tensor form. Derivation can be found in (Versteeg and Malalasekera, 2007; Toro, 2009).

$$\frac{\partial \boldsymbol{U}}{\partial t} + \nabla \cdot \boldsymbol{F} - \nabla \cdot \boldsymbol{G} = \boldsymbol{H}$$

Equation 4: Where **U** are the conserved variables, **F** and **G** are the advective and diffusive terms respectively and **H** are source terms.

$$\boldsymbol{U} = [\rho, \rho u, \rho v, \rho w, \rho E]^T$$

$$\boldsymbol{F} = \begin{bmatrix} \rho u & \rho v & \rho w \\ \rho u^2 + p & \rho uv & \rho uw \\ \rho uv & \rho v^2 + p & \rho vw \\ \rho uw & \rho vw & \rho w^2 + p \\ u(\rho E + p) & v(\rho E + p) & w(\rho E + p) \end{bmatrix}$$

$$\mathbf{G} = \begin{bmatrix} 0 & 0 & 0 \\ \tau^{xx} & \tau^{yx} & \tau^{zx} \\ \tau^{xy} & \tau^{yy} & \tau^{zy} \\ \tau^{xz} & \tau^{yz} & \tau^{zz} \\ u\tau^{xx} + v\tau^{xy} + w\tau^{xz} - C_p \dfrac{\mu}{Pr} \dfrac{\partial T}{\partial x} & u\tau^{yx} + v\tau^{yy} + w\tau^{yz} - C_p \dfrac{\mu}{Pr} \dfrac{\partial T}{\partial y} & u\tau^{zx} + v\tau^{zy} + w\tau^{zz} - C_p \dfrac{\mu}{Pr} \dfrac{\partial T}{\partial z} \end{bmatrix}$$

Equation 5: Where ρ is the density, u, v and w are the x, y and z components of velocity respectively, E is the energy, p is the pressure, τ^{ij} is the viscous stress in ij direction, C_p is the specific heat at constant pressure, μ is the dynamic viscosity, Pr is the prandtl number and T is the temperature.

$$\tau^{ij} = 2\mu\left(S_{ij} - \frac{1}{3}\frac{\partial u_i}{\partial x_i}\delta_{ij}\right) \qquad S_{ij} = \frac{1}{2}\left(\frac{\partial u_i}{\partial x_j} + \frac{\partial u_j}{\partial x_i}\right)$$

Equation 6: Where δ_{ij} is defined as 1 if i = j and 0 if i ≠ j, **S** is the strain rate tensor with the ijth term being S_{ij}.

$$\mathbf{H} = \begin{bmatrix} 0 \\ \rho g_x + F_{ext_x} \\ \rho g_y + F_{ext_y} \\ \rho g_z + F_{ext_z} \\ \rho \boldsymbol{V} \cdot \boldsymbol{F}_{ext} \end{bmatrix}$$

Equation 7: Where g_i is the gravitational acceleration in the ith direction, $\mathbf{F_{ext}}$ is the external force vector and **V** is the velocity vector.

It is common to time-average the equations, also called Reynolds Averaging, leading to the Reynolds Averaged Navier-Stokes equations (RANS). What this means is that the variables are represented as a mean and a fluctuating component. When this is applied to the Navier-Stokes equations a Reynolds stress tensor emerges which is due to the fluctuating component of the flow.

$$\boldsymbol{G}^{RANS} = \begin{bmatrix} 0 & 0 & 0 \\ \tau_t^{xx} & \tau_t^{yx} & \tau_t^{zx} \\ \tau_t^{xy} & \tau_t^{yy} & \tau_t^{zy} \\ \tau_t^{xz} & \tau_t^{yz} & \tau_t^{zz} \\ u\tau_t^{xx} + v\tau_t^{xy} + w\tau_t^{xz} - C_p \dfrac{\mu_t}{Pr_t} \dfrac{\partial T}{\partial x} & u\tau_t^{yx} + v\tau_t^{yy} + w\tau_t^{yz} - C_p \dfrac{\mu_t}{Pr_t} \dfrac{\partial T}{\partial y} & u\tau_t^{zx} + v\tau_t^{zy} + w\tau_t^{zz} - C_p \dfrac{\mu_t}{Pr_t} \dfrac{\partial T}{\partial z} \end{bmatrix}$$

Equation 8: Where the RANS components ($\mathbf{G}^{RANS}$) are similar to those in the diffusive fluxes except with their respective turbulent quantities.

$$\tau_t^{ij} = 2\mu_t\left(S_{ij} - \frac{1}{3}\frac{\partial u_i}{\partial x_i}\delta_{ij}\right) - \frac{2}{3}\rho k \delta_{ij}$$

Equation 9: Where μ_t is the turbulent dynamic viscosity and k is the turbulent kinetic energy.

The values of μ_t and k need to be calculated. This is done by the introduction of turbulence models.

Turbulence models

Since there is no way of knowing what the values for the turbulent dynamic viscosity and the turbulent kinetic energy will need to be beforehand, they need to be calculated. It is here where the introduction of the turbulence model comes in. All turbulence models are used to

calculate these two turbulence quantities or the Reynolds stress terms. The method of achieving these varies; some models can be mixing length models, two equation models or Reynolds stress models which solve seven extra equations. Two equation models have been considered here as they are commonly used in industry due to good accuracy and little solution cost increase.

Two equation models

There are many two equation models available to use for the prediction of turbulence, the most common are the k-Epsilon, the k-Omega and the k-OmegaSST. All of these models solve a transport equation for the turbulent kinetic energy k, and one other constant.

k-Epsilon

The k-Epsilon equation was first introduced in (Jones and Launder, 1972). This model describes a transport equation for the turbulent kinetic energy k, and another for the turbulent dissipation rate ε. Various combinations of these variables are enough to form dimensioned variables which represent the unknown terms in the Reynolds stress tensor. This model is considered complete as there need be no prior information of the flow before simulation.

As discussed in (Pope, 2015) there are drawbacks to this turbulence model as it has poor performance in strong pressure gradient flows and also requires yPlus meshes of above 15. As such wall functions must be used with the standard model. Low Reynolds number models are available where yPlus meshes of 1 are suitable. The use of wall functions can severely under predict separated flow and the exact separation points within the flow. However this model does perform well in the far field with good prediction of the transport of vortices.

k-Omega

The common version of this model was proposed in (Wilcox, 1988). This model also describes a transport equation for the turbulent kinetic energy k, and another for the specific dissipation rate ω. As with the k-Epsilon equation various combinations of these variables form the dimensioned variables in the Reynolds stress tensor. Again this model is considered complete as no prior information about the flow is required prior to simulation.

As discussed in (Pope, 2015) this model is superior to the k-Epsilon equation in the viscous sublayer and flows with pressure gradients. This results in meshes of yPlus of around 1 to be able to be used without the need for wall functions and as such is able to predict separation accurately. This model however, performs poorly in the free stream as the calculated value is very sensitive to the condition imposed on the free stream boundary. This leads to the solver inaccurately predicting the transport of vortices into the domain.

k-OmegaSST

First proposed by (Menter, 1994) this model is a blend of the k-Epsilon, which is transposed into an ω equation in the free stream and k-Omega in the near wall region. Therefore this model takes the best from each which is why the following model will be used.

$$\frac{\partial(\rho k)}{\partial t} + V \cdot \nabla \cdot (\rho k) = P_m - \beta^* \rho \omega k + \nabla \cdot [(\mu + \sigma_k \mu_t) \nabla k] + \beta^* \rho \omega_{amb} k_{amb}$$

$$\frac{\partial(\rho \omega)}{\partial t} + V \cdot \nabla \cdot (\rho \omega) = \frac{\gamma_m}{\nu_t} P_m - \beta \rho \omega^2 + \nabla \cdot [(\mu + \sigma_\omega \mu_t) \nabla \omega] + 2(1 - F_1) \frac{\rho \sigma_{\omega 2}}{\omega} (\nabla k \cdot \nabla \omega) + \beta^* \rho \omega_{amb}^2$$

$$P_m = \mu_t \Omega_v^2 - \frac{2}{3}\rho k \delta_{ij} \frac{\partial u_i}{\partial x_i}$$

$$\mu_t = \rho k T$$

$$T = min\left[\frac{a_1}{\max(a_1\omega, \Omega_v F_2)}, \frac{0.6}{\sqrt{3}\Omega_v}\right], \quad \Omega_v = \sqrt{2W_{ij}W_{ij}}, \quad W_{ij} = \frac{1}{2}\left(\frac{\partial u_i}{\partial x_j} - \frac{\partial u_j}{\partial x_i}\right)$$

Where each of the variables (σ_k, σ_ω, γ_m and β) are blended using the following function.

$$\phi = F_1\phi_1 + (1 - F_2)\phi_2$$

$$F_1 = \tanh(arg_1^4)$$

$$arg_1 = min\left[max\left(\frac{\sqrt{k}}{\beta^*\omega d}, \frac{500\nu}{d^2\omega}\right), \frac{4\rho\sigma_{\omega 2}k}{max\left(2\rho\sigma_{\omega 2}\frac{1}{\omega}\frac{\partial k}{\partial x_j}\frac{\partial \omega}{\partial x_j}, 10^{-20}\right)d^2}\right]$$

$$F_2 = \tanh(arg_2^2)$$

$$arg_2 = max\left(2\frac{\sqrt{k}}{\beta^*\omega d}, \frac{500\nu}{d^2\omega}\right), \qquad \gamma_1 = \frac{\beta_1}{\beta^*} - \frac{\sigma_{\omega 1}\kappa^2}{\sqrt{\beta^*}}, \qquad \gamma_2 = \frac{\beta_2}{\beta^*} - \frac{\sigma_{\omega 2}\kappa^2}{\sqrt{\beta^*}}$$

$$\sigma_{k1} = 0.85, \sigma_{k2} = 1.0, \ \sigma_{\omega 1} = 0.5, \ \sigma_{\omega 2} = 0.856, \beta_1 = 0.075, \beta_2 = 0.0828, \beta^* = 0.09, \kappa = 0.41, a_1 = 0.31$$

Equation 10: Description of the k-OmegaSST turbulence model with closure coefficients. Variables are as previously described, with d being the wall distance.

Density vs pressure based solvers

Having described which equations are going to be solved, where the pressure field is also unknown beforehand, coupling between calculated variables and pressure is required. There are different approaches to how the pressure field is calculated based on compressible (density based) and incompressible (pressure based) formulations.

Density based

Density based solvers require a coupling between density, temperature and pressure; this comes from an equation of state. There are various equations of state based on material used and solvers chosen. They are of the common form shown below.

$$p = p(\rho, T)$$

Equation 11: Showing that the pressure is a function of density and temperature

With this the system can be solved. Benefits of the density based solvers are that they are capable of simulating high speed flows with or without preconditioning, and are capable of solving low speed flows with sufficient preconditioning. All of the usual acceleration techniques can be used such as geometric multigrid and dual time-stepping to help convergence.

Pressure based

Unlike density based solvers, pressure based solvers do not solve the energy equation but instead solve an elliptic equation for pressure that is derived from discretising the momentum equation.

$$\nabla \cdot \left(\frac{\nabla p}{a_p}\right) = \nabla \cdot \left(\frac{\boldsymbol{H}(\boldsymbol{u})}{a_p}\right)$$

$$H(u) = r - \sum_f a_f u_f$$

Equation 12: Poisson equation for pressure.

Pressure based methods involve a predict and correct method for solving the flow. Drawbacks include that the method derived does not account for the phenomenon of compressibility at high speeds unless reformulated and could lead to the under prediction of shock waves within the flow.

3.5. Post processing

There are many methods of generating usable data from CFD simulations. Two common methods are lift and drag coefficients and also the coefficients of pressure plots which are used to compare against experimental data. Others include contours of Q-criterion, streamlines and surface line integral convolution (LIC) which are used as a visualisation of the flow field.

Drag coefficients

The following formula can be used to calculate the drag coefficient.

$$C_d = \frac{F_d}{\frac{1}{2}\rho U^2 A}$$

Equation 13: Where F_d is the drag force, C_d is the drag coefficient, ρ is the fluid density, U is the free stream velocity and A is the reference area.

Forces on a body can be broken down into two categories, pressure and viscous drag. They both are accounted for below which are summations over all faces making up the body under investigation.

$$\boldsymbol{F} = \sum_f pA\boldsymbol{n} + \sum_f 2\mu A\boldsymbol{S}\cdot\boldsymbol{n}$$

Equation 14: Where **F** is the force vector, p is the pressure, A is the area of the face, **n** is the face normal, μ is the dynamic viscosity and **S** is the strain rate tensor.

Again the area, free stream velocity and lift and drag direction are supplied to the solver.

Coefficient of pressure

As with the lift and drag coefficients coefficient of pressure can be calculated.

$$C_p = \frac{p - p_\infty}{\frac{1}{2}\rho U^2}$$

Equation 15: Where C_p is the coefficient of pressure, p is the local pressure, p_∞ is the free stream pressure, ρ is the density and U is the free stream velocity.

This compares the ratio between static pressure and dynamic pressure.

Q-criterion

One method for visualising is to contour the q-criterion. The q-criterion is defined below.

$$Q = \frac{1}{2}[|\boldsymbol{\Omega}|^2 - |\boldsymbol{S}|^2] \qquad \boldsymbol{\Omega} = \frac{1}{2}[\nabla \boldsymbol{u} - (\nabla \boldsymbol{u})^T] \qquad \boldsymbol{S} = \frac{1}{2}[\nabla \boldsymbol{u} + (\nabla \boldsymbol{u})^T]$$

Equation 16: Where Q is the Q-criterion, **Ω** is the vorticity tensor, and **S** is the strain rate tensor.

This can be used to visualise the vortex core, which in turn can be used to visualise the flow field around an object.

Streamlines and surface LIC

Streamlines and surface LIC are other methods of visualising the flow. Streamlines represent a 3D representation of the flow, whereas the surface LIC represents flow bound to the surface. Surface LIC is used to show the surface shear stresses and also oil flow patterns. Suppose there is a massless particle of fluid, the streamline is the path traced out by this massless particle being moved by the flow.

4. Experimental investigation

In order to fully investigate the geometry to the highest detail it is recommended to increase the level of detail from the simplest case up to the highest detail case in increments. This is capable of being investigated as the geometry is modular, several of the modules can be exchanged which alters the level of detail in the model.

In order to focus the project one rear body configuration was chosen. The three choices were the fast-back, notch-back and estate-back. The fast-back was chosen as it represents similar geometry to the Ahmed body and should include similar flow features. Three levels of detail were investigated as this was considered to cover the largest amount of configurations in the minimum number of cases investigated. All geometry was provided and hence no geometry generation was needed.

In order for the solution to be stopped, convergence criteria have to be defined. This usually is taken when the residuals drop below a certain value, while this is true there are often cases where the forces on a body converge much before the residuals do. For this case there is an intermediate approach taken. That intermediate approach being that the forces must have converged but also the residuals must be below $1x10^{-3}$.

4.1. Solvers investigated

As there are a variety of solvers available, some being commercial others being open source, three were investigated. zCFD solver is available from Zenotech, Fluent is available from ANSYS, and OpenFOAM is open source.

zCFD

zCFD is a highly parallel unstructured finite volume solver capable of running on CPU, along with GPU or Intel Xeon PHI hardware acceleration. zCFD is a density based solver with Weiss-Smith low Mach number pre-conditioning. zCFD was written with parallelism in mind from the outset. Along with multigrid acceleration, steady and unsteady dual time-stepping zCFD represents a highly efficient industry standard code.

With recent developments in numerical methods zCFD has implemented a Nodal Discontinuous Galerkin (Nodal DG) with Flux Reconstruction (FR) High Order (HO) solver.

Fluent

Being part of a suite of engineering design tools, Fluent is also a typical industrial CFD solver. With the choice of pressure or density based solvers for low and high Mach number flows respectively Fluent is capable of solving many industrial CFD problems. Also the k-OmegaSST turbulence model has been implemented meaning that there can be comparison between the solvers as they solve the same equations.

Fluent is also capable of running in parallel along with taking advantage of the GPU acceleration. Fluent can also be run with and without a GUI.

OpenFOAM

OpenFOAM (Open Field Operation and Manipulation) engineering toolbox has the capability to solve a wide range of industrially relevant flow, from combusting to electromagnetics. The majority of OpenFOAM is parallel allowing the use of developments in computing hardware. Being open source OpenFOAM's codebase allows for the user to implement their own models which means that OpenFOAM is more versatile than the industrial codes.

With many solvers and numerical methods implemented OpenFOAM allows full control over the solution methods used.

4.2. Initial conditions

Initial conditions are vital, along with boundary conditions, for the accuracy of any CFD simulation. The boundary and initial conditions used must be as close as possible to those used for the experiment. As the experiment by TUM was conducted in a wind tunnel the exact conditions can be measured and used.

Table 1: Showing the initial conditions from the experiment

Condition	Value
Velocity	$16 m.s^{-1}$
Reference Length	4.6m
Reynolds Number	$4.86x10^{6}$
Reference Area	$2.15m^{2}$
Wheel angular velocity	$50.69 rad.s^{-1}$

These values were inserted into the input files for the three codes being used. Those three codes being used are zCFD, Fluent and OpenFOAM.

4.3. Case 1

The details for the initial investigation case were that there were no wheels, a smooth underbody and no wing mirrors. This geometry represents a similarity to the Ahmed body due to the smooth underbody and the rear geometry. The main difference is that the Ahmed body contains wheel-like geometry whereas the initial case does not. However this initial

case includes more industrially relevant detail than that of the Ahmed body and therefore is more industrially relevant.

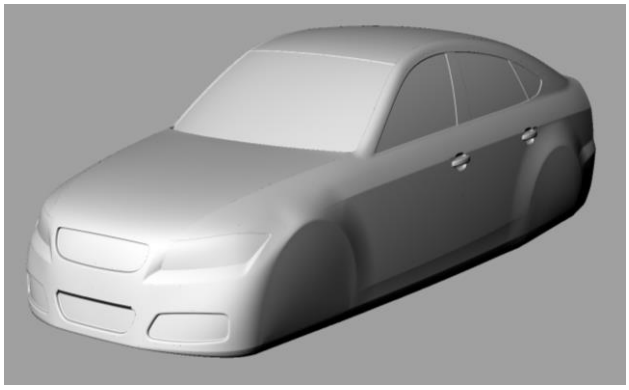

Figure 1: Showing the geometry for case 1.

One main reason why this geometry will stress the turbulence models is that there is expected, as with the Ahmed body, to be some vortices generated by the rear bodywork along with separation, shear layers and acceleration to the flow from various regions of the geometry. This will test the k-Omega formulation with pressure gradients, and also the transition to the k-Epsilon equation in the freestream and the transport of vortices.

As the initial investigation case many of the processes that needed to be undertaken to achieve a solution were inefficient. Initial attempts at CAD clean-up had been very time consuming. This was partly due to inexperience with the software used, but also grasping topological concepts that are required for describing geometry. Throughout the process the efficiency increased.

The geometry provided needed some cleaning as some of the surfaces had duplicate edges and gaps between them. These edges were merged without impacting on the underlying geometry too much.

Following this the mesh for the geometry could be produced. This involved creating the surface mesh. This surface mesh needed some refining as the criteria were above the recommended levels. Once the mesh was of sufficient quality, the volume mesh could be produced.

Creating the volume mesh initially involved creating the volume domain. To be functional and not impact the solution, the boundaries had to be placed sufficiently far enough away from the geometry. The inlet was placed 3 car lengths in front, the sides were placed 2 car lengths either side, the top was placed two car lengths away and finally the outlet was placed 10 car lengths away. The outlet was placed this distance away to enable the wake of the car to dissipate out and return to free stream velocity. This domain was used for each and every case investigated to ensure consistency between the cases.

For the specific turbulence model the yPlus value of the mesh could be around 1. This led to the specification of the yPlus in the mesh generator that then grew boundary layer cells from the walls to fully capture the boundary layer profile.

Having produced a volume mesh, some of the surface mesh needed to be altered as it led to some of the mesh criteria being above the recommended values. These areas were altered and the volume was re-meshed, generating a mesh that passed the quality checks.

Having produced a mesh that passed the quality criterion checks it could be exported into the three solver formats that were used.

4.4. Case 2

This case developed on the initial investigation case; this was done by the introduction of the wheel geometry. As there are three wheel configurations the simplest is a smooth tyre surface and no alloys, the next being smooth tyre surface with alloys and the most detailed being the treaded tyre surface with alloys. As this was the intermediate detailed case, the smooth tyre surface with alloy configuration for the wheels was chosen.

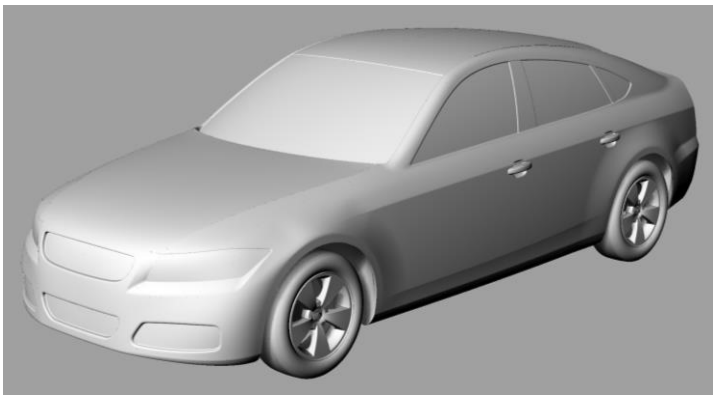

Figure 2: Showing the geometry for case 2.

Further to the vortices generated from the rear body configuration, this case would introduce shear layers. These shear layers would appear at the wheel arches. Along with these there would be rotating geometry which would test the solvers implementation of rotating geometry and the associated flow regime.

As with the initial case the geometry needed CAD cleaning. For this case, as there was an increased number of surfaces, clean-up took a little while longer. It was noticed that the wheel geometry was identical for each of the four wheels present. Time was saved by cleaning one wheel geometry and duplicating this cleaned geometry in all of the four corners.

With the introduction of the wheel geometry there developed some meshing issues. Typically mesh generators have difficulty in generating high quality meshes from geometry with grazing angles. There were regions where this was an issue. They were where the four tyres met the road surface. It was therefore investigated and one conclusion that was reached was that tyres have contact patches in reality.

To solve this a contact patch was created by cutting the tyre geometry which adequately represented a contact patch. Other methods considered included placing the tyre on a block which raised it up and alleviated the issue. This method was deemed to be too far removed from the reality. It was decided that the contact patch method would be used as the fundamental reasoning was based on that of reality, and as this geometry is more industrially relevant then the modelling practices should be as close to reality as possible.

Following the contact patch creation the surface mesh along with the volume mesh could be created. Ensuring that the quality parameters were below the recommended values required some iterative refinement. As with case 1 the mesh was exported into the relevant formats for the solvers used.

Figure 3: Showing the grazing angle.

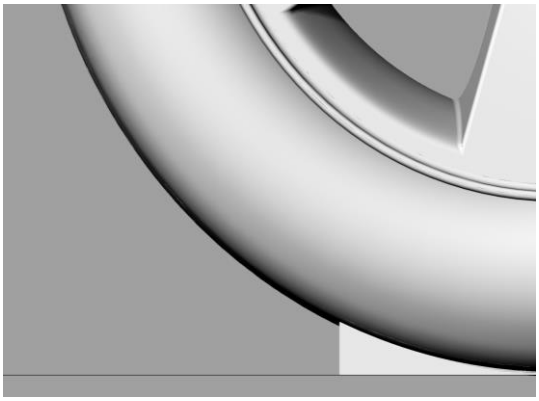

Figure 4: Showing the block method.

Figure 5: Showing the contact patch approach.

4.5. Case 3

Adding further detail to case 2 resulted in the geometry simulated having a high relevance to industry. This final case added a detailed underbody, detailed wheels, exhausts and also wing mirrors to the geometry. In this, underfloor effects can be investigated as the underbody is simulated to an adequate level of detail.

Due to the increase of the number of surfaces, there undoubtedly would be an increase of the number of gaps in the surfaces. This added detail led to an increase in the time taken to clean the whole geometry.

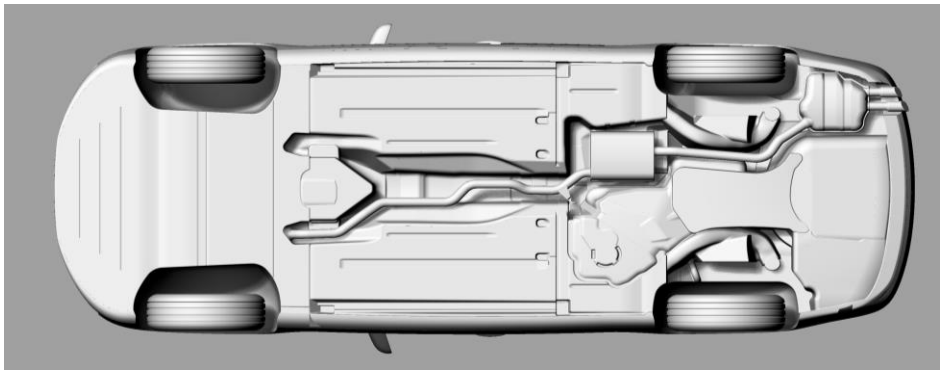

Figure 6: Showing the detail on the underbody.

Further to that of case 2 this model introduces more detail, which should introduce an increase of the shear layers, vortices and a more complex flow regime, solely due to the increase of detail. With the introduction of wing mirrors there may be a possibility of periodic vortex shedding. An aero-acoustic investigation could be conducted into the noise produced by the vortices shedding.

Again, as with case 2, the wheels geometry was given a contact patch which helped with the meshing. There were also more difficulties in meshing the detailed geometry. The reason why these difficulties arose was due to there being increased detail resulting in difficulties generating cells that had low skewness.

However, following some refinement, meshes were able to be produced which fell below the required quality criterion. Once this had been achieved the meshes were exported to the required formats for the solvers.

5. Presentation of results

All experimental results are taken from (Heft *et al.* 2012 (b)).

5.1. Case 1

Mesh independence study

In order to be able to rely on the accuracy of the results from the CFD simulation a mesh independence study must be conducted. This involves creating various meshes with a decreasing cell size. By doing this it can be seen where the mesh cell size had no impact on the solution. This will be investigated and mesh independence will be considered when the drag coefficient is independent of the cell size.

Table 2: Showing results for a mesh independence study using zCFD.

Number of cells	Drag coefficient
4.5 million	0.095
9 million	0.109
13 million	0.115
18 million	0.1152

By completing a mesh independence study the results can then be validated against the experimental data. From the table it can be seen that the 13 million cells is the cut off for the mesh independence. Therefore this mesh will be taken forward.

Mesh Quality

Having conducted a mesh independence study the mesh that was considered independent was taken forward. In order to ensure that the mesh is of decent quality the mesh statistics have been tabulated.

Table 3: Showing the mesh quality results.

Mesh Statistic	Average value
Skewness	0.75
Orthogonality	0.5
Volume ratio	125
yPlus	0.89

Drag coefficient

Having deduced that the mesh has a good quality, the calculation of the drag coefficient for each of the solutions produced by the three solvers has been tabulated.

Table 4: Showing the drag coefficient results from each solver.

Solver	Drag coefficient	Percentage error (%)
Experimental	0.115	-
zCFD	0.115	0
Fluent	0.115	0
OpenFOAM	0.175	52

Coefficient of pressure

In order to further validate the codes the plots for the coefficient of pressure are taken, as with the experiment, down the centre of the car. These are plotted for each solver on the same plot as the experimental data.

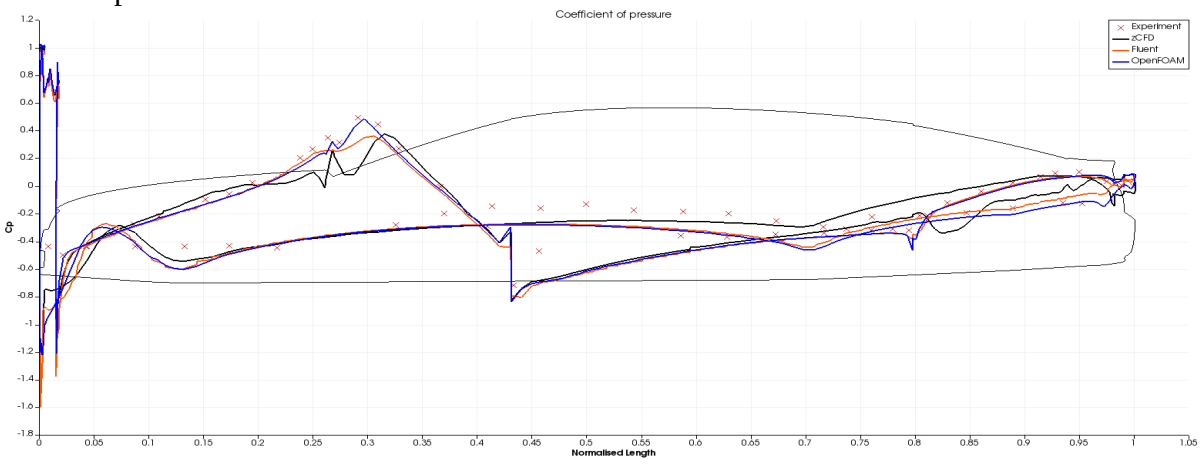

Figure 7: Showing the coefficient of pressure results along with the experimental.

Core hours

As efficiency and carbon footprint are an important issue there is an increased demand for efficient solvers. Therefore the time taken for the solution in total number of core hours was recorded during the simulation.

Table 5: Showing the number of core hours for solution

Solver	Core hours
zCFD	2304
Fluent	2336
OpenFOAM	3240

5.2. Case 2

Mesh quality

As for the previous case a mesh independence study was investigated. The outcomes being that the mesh to be independent contained 16 million cells, an increase over the previous case. This increase was partly due to the introduction of the wheels and its associated details.

Due to this increase in cell count the mesh quality did improve, as shown with the results tabulated below.

Table 6: Showing the different mesh qualities.

Mesh Statistic	Average value
Skewness	0.72
Orthogonality	0.55
Volume ratio	124
yPlus	0.89

Drag coefficient

Allowing the simulations to converge, and as with the previous case, the drag coefficient could be extracted and compared with the experimental data. They can be seen below.

Table 7: Showing the drag coefficient results for each solver.

Solver	Drag coefficient	Percentage error (%)
Experimental	0.233	-
zCFD	0.2312	0.77
Fluent	0.2259	3.05
OpenFOAM	0.2792	19.87

Coefficient of pressure

Again, as in the previous case, the coefficients of pressure plots for the centre line of the car have all been plotted together on the same diagram.

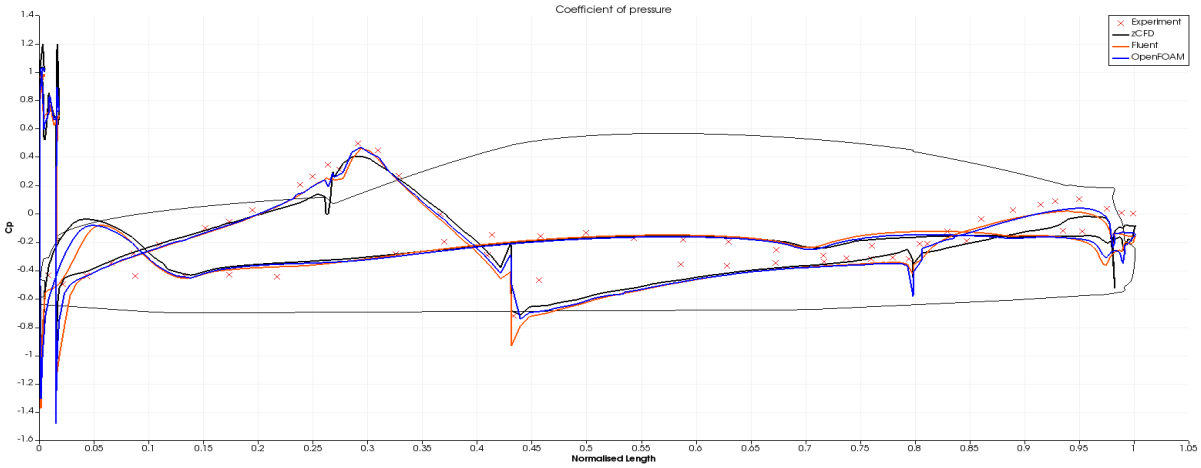

Figure 8: Showing the coefficient of pressure along with experimental results.

Core hours

As this case had an increased number of cells along with slightly more complex flow, due to the wheel geometry, there was an increase in the time taken to convergence. This led to an increase in the number of core hours taken.

Table 8: Showing the number of core hours for convergence.

Solver	Core hours
zCFD	2448
Fluent	2521
OpenFOAM	3840

5.3. Case 3

Mesh Quality

Again, as with the previous cases, a mesh independence study was conducted. There was a large increase in cell count to allow for the capture of the increased details of the geometry. With this the mesh that was considered contained 66 million cells.

This increase is also due to the need for a high resolution in some areas of the geometry due to the high curvature added by the increased detail. As there was an increased amount of detail there was difficulty in generating high quality cells, however the general guidelines have been adhered to in order to generate reliable solutions.

Table 9: Showing the results for the mesh statistics.

Mesh Statistic	Average value
Skewness	0.81
Orthogonality	0.63
Volume ratio	132
yPlus	0.89

Drag coefficient

As this case is most similar to that of the real world case the results are of interest and help validate a CFD code. Again the drag coefficients for each of the CFD codes used have been tabulated below.

Table 10: Showing the calculated drag coefficient.

Solver	Drag coefficient	Percentage error (%)
Experimental	0.278	-
zCFD	0.2794	0.51
Fluent	0.273	1.80
OpenFOAM	-	-

Coefficient of pressure

As with the previous two cases the coefficient of pressure along the car centreline is plotted against the experimental data.

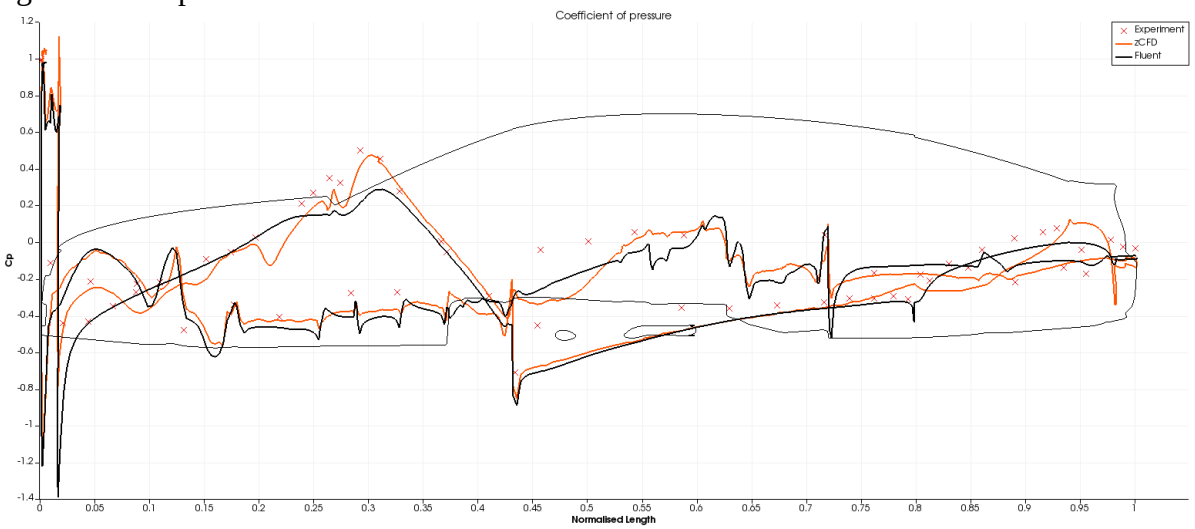

Figure 9: Showing the results for coefficient of pressure along with experimental.

Core hours

Again due to the increase of complexity of the flow solution along with the increased number of cells present the time taken for convergence was increased. This led onto an increase in the total number of core hours needed to solve this case.

Table 11: Showing the number of core hours to convergence.

Solver	Core hours
zCFD	6480
Fluent	7568
OpenFOAM	-

5.4. Overall flow regime

Although the coefficient of pressure and drag values give good insight as to the accuracy of the solver they do not show if a physically realistic flow field is being produced. Therefore an investigation of the velocity field need be conducted.

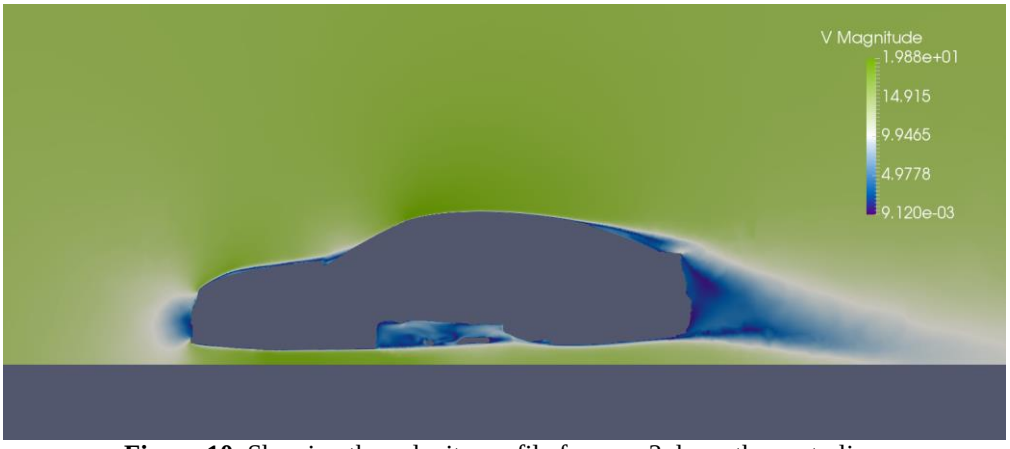

Figure 10: Showing the velocity profile for case 3 down the centreline.

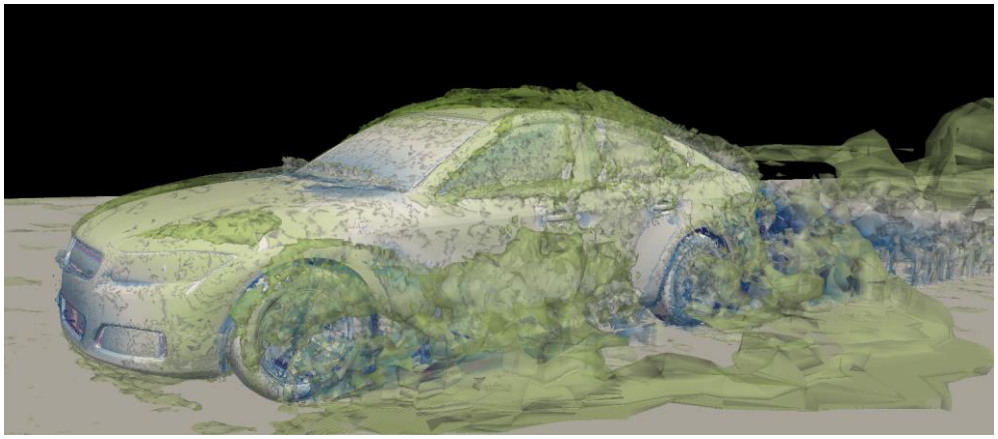

Figure 11: Showing a Q-criterion plot for case 2 which shows similar flow regime to the other cases.

6. Discussion and conclusions

6.1. Case 1

Mesh

All solvers are using the same mesh, which is the mesh shown to give a solution that is mesh independent, and as such all differences experienced in solution would result from numerical implementations and differences in the code. However it is still worth reviewing the mesh quality statistics. yPlus values for the mesh are required for the k-OmegaSST model and therefore are governed by this. The yPlus required is of order 1, the mesh generated has an average yPlus of 0.89. This is of the correct order of magnitude and should not have too much of an impact on the solution, along with being suitable for the turbulence model to be used without wall functions. The volume ratio value of 125 is around an acceptable value and relates to a gradual gradient from small to large cells.

The skewness and orthogonality of the mesh are below the maximum values that are accepted as the worst case for that criterion. From this the mesh can be considered average quality. It is clear that to generate a high quality mesh a large amount of time will need to be invested into the meshing process or a large number of cells are required. However as this investigation is about developing an industrially relevant test case, time is limited in industry and therefore high quality meshes are rarely produced. Therefore solvers must be able to generate adequate results on average quality meshes.

Drag Coefficient

From the tabulated data it can be seen that both zCFD along with Fluent are able to capture the experimental value for the drag coefficient at 0.115. OpenFOAM on the other hand has an error of around 50%. This error from OpenFOAM may be related to an implementation of the turbulence model or some error in the force calculation. One drawback about only comparing the coefficients is that it is unable to determine if the correct flow field is being calculated as there are no results for the wake profile. However, as the correct drag value was calculated, it seems likely that there will be similarities between the experiment and computed wake.

As two of the solvers investigated generated the results with little error this suggests that the mesh is of adequate quality and that the generally accepted values for the mesh quality do not have a large impact on the solution. These quality criteria will still be used as maximum values in the other cases.

Coefficient of pressure

There are discrepancies between the calculated and experimental pressure coefficients; however the general trend is recovered. There is an under predication in the peak located at x = 0.3 for both zCFD and Fluent. OpenFOAM seems to capture this exactly. This peak is caused by the shear layer from the car bonnet impacting the windscreen, causing a high pressure.

zCFD better predicts the suction at x = 0.7, whereas OpenFOAM and Fluent over predict this value. It can be seen that the solvers do have the general trend and each one is particularly accurate in different regions. This could be due to the implementations of the equations within the code responding better to different flow areas.

All of the solvers seem to be able to capture a large drop in pressure at x = 0.43. This also matches the experimental trend in this region. This region relates to the flow over where the windscreen joins with the roof. This drop relates to the acceleration of the flow caused by this angle change and the coanda effect. The coanda effect relates to the ability of a fluid to stick to a surface. As over the roof this surface is curved, this accelerates the flow, leading to a decrease in pressure. This accelerated flow explains why there is a decrease in the coefficient of pressure immediately following this large drop in pressure. The solvers seem to over predict this acceleration of the flow.

zCFD under predicts in the region of x = 0.8 to x = 0.95. This relates to the solver predicating an increased separation in this region above the other solvers and as such a lower pressure is observed. All solvers predict fairly accurately the coefficient of pressure at the very rear of the car in the wake region.

Experimental data that has been provided is coarse, in that there could be more data points for comparison. This would lead to a better comparison between the simulated and experimental results giving CFD codes better validation, and possible insight into where the models are under or over predicting flow. Even with this slight difference between the simulation and the experiment plots the drag coefficient is still captured.

Core hours

It can be seen that to achieve a similar level of accuracy zCFD is the most efficient for the same mesh. It can be seen that the two commercial codes perform much more efficiently than that of the open source code. This may be due to the pressure that the commercial customers put on the developers for efficiency and a reduced cycle time. This would lead to zCFD having the lowest power consumption and carbon footprint of all of the solvers.

6.2. Case 2

Mesh

Mesh independence was achieved at around 16 million cells. The yPlus value and volume ratio values are similar to those of the previous case and also below the recommended value. This is due to them being specified at the meshing stage, which was consistent between the three cases. Also the yPlus value would be suitable to use with the turbulence model without wall functions.

There was an increase in the number of cells, which was partly related to the increased detail of the wheels, but also due to there being a general decrease in cell size. This led on to the cells having an improved quality over those in the previous case. Improved quality meshes give better quality results, which have less numerical error than those of a poor quality mesh.

Drag coefficient

As with the previous case, and with increased detail from the wheels, zCFD and Fluent are able to capture the drag coefficient to within a reasonable degree of accuracy. zCFD had 0.77% error and Fluent had 3.05% error from the experimental value of 0.233. The error introduced could be due to the assumptions made with the contact patch assumption with the wheels. This assumption would alter the flow regime a little which would propagate throughout the domain and possibly influence the overall flow and impact the drag.

As before OpenFOAM was unable to capture the drag coefficient to within a reasonable degree of accuracy. This may be a recurring issue which could also be present in the initial case.

Coefficient of pressure

As before the three solvers accurately capture the general form of the experimental data across the whole car. All of the plots also agree very closely to those of the experiments as they all are able to capture the peak at x = 0.3 to within a good degree of accuracy. This is caused by the shear layer originating from the end of the car bonnet. This shear layer then impacts the windscreen causing an increase in pressure in this region accounting for the peak.

The solvers do seem to over predict the acceleration caused by the curved roof of the geometry in the x = 0.425 region, as seen by the solver coefficients being lower than

experimental showing an increase in the predicted acceleration leading to a decrease in pressure. This acceleration is due to the coanda effect described earlier. Again this over prediction in acceleration impacts immediately after and is present until x = 0.64 where the flow again agrees with the experimental data.

There is a peak at x = 0.05 that solvers predict whereas the experimental data does not. This peak may suggest that solvers are predicting an increase in stagnation pressure over that of the experiment.

There is an over prediction with zCFD in the region x = 0.85 to x = 0.95. This over prediction results from zCFD predicting an increased level of separation whereas Fluent and OpenFOAM do not. This has also been predicted in case 1 by zCFD only. Immediately prior to this zCFD does predict a sharper drop in the coefficient of pressure. This sharp drop may trip the boundary layer to separate resulting in a decreased pressure downstream, whereas Fluent and OpenFOAM predict a smoother drop which would result in less separation.

Core hours

As with the previous case zCFD is the most efficient. Along with this an increase of 3 million cells does not relate to there being a significant time increase. Also, as before, the commercial codes show better efficiency than that of the open source software. Again zCFD would have the lowest power consumption of the three and as a result lower computational cost.

6.3. Case 3

One point to note is that the OpenFOAM simulation was unable to run. The same input files that were previously used for case 2 were copied and used on case 3. A discussion on why follows.

Mesh

As with the previous two cases the yPlus and volume ratio remained around the same value for the mesh that was considered mesh independent. An increase of the number of cells was seen to around 66 million. This was mainly due to the increased detail of the case requiring a large number of cells to fully capture the surface gradients accurately both in the tyre tread and the underfloor. The mesh qualities also remained below the maximum values as with the previous two cases.

Drag Coefficient

An increase of detail led to there being greater error between the solvers and experimental results. However there is still good agreement of the simulated and experimental data, the maximum error for zCFD and Fluent are 0.51% and 1.80% respectively from the experimental value of 0.278. This level of accuracy for an industrially relevant geometry is promising.

It was believed prior to this that the increase of detail would lead to an increased error. This would be due to the increased modelling assumptions made, along with the surface discretisation leading to inaccuracies with the simulated geometry and the experimental geometry.

Coefficient of pressure

As before the general trend of the flow are captured. However, with the increase of detail there are some differences in the plots. zCFD captures the peak at x = 0.3 along with the detail around that region. Fluent under predicts the peak in this region which could be related to there being simulated a decrease in separated flow impacting the windscreen in this region.

As before the solvers capture the suction at x = 0.425. Similarly, the solvers seem to over predict the coanda effect, the acceleration of the flow, over the roof which propagates downstream. As before zCFD predicts increased separated flow over the region of x = 0.8 to x = 0.88 shown by the lower coefficient of pressure. Fluent appears to simulate less separation in the flow, which results in a greater pressure coefficient shown.

Similar to case 1 and 2 zCFD predicts increased boundary layer separation at the point x = 0.8. This leads to a reduction in the value of the coefficient of pressure at these regions. Fluent does not capture this, predicting decreased separation of flow, and as such has higher values in this region.

There is a very noisy coefficient of pressure plot on the bottom surface which the experimental results do not seem to show. This could be caused by aliasing of the experimental results. To improve the comparison ideally more data points would be used to capture these fluctuations if present in the experiment. This is due to the increase in detail causing separation and shear layers throughout the whole length. However the general trend coefficients of pressures of the two solvers are in good agreement with the experimental data.

It is clear from the noisy behaviour of the plots that there is a high amount of turbulence exhibited on the underside of the car. As would be expected, this is related to there being a large amount of detail from the geometry causing separated flow and shear layers.

Core hours

As before there is an increase in solution time. However there is a significant difference between the solvers. zCFD is around 14% more efficient. This difference was not noticeable at low cell counts but can be seen at higher ones. This leads onto zCFD giving a more accurate solution at a lower core hour time. As before zCFD would have the lowest power consumption.

6.4. Overall flow regime

Conclusions drawn from the pressure plots can be seen in the velocity profile of case 3. That is to say that the shear layer impacting the windscreen causing the pressure peak in the coefficient of pressure plots can be seen. Also the acceleration due to the coanda effect can be seen over the top of the roof by the increase in the velocity in this region. Separated flow of the rear window can also be seen as predicted when analysing the coefficient of pressure plots. These flow phenomena are expected throughout each of the cases as these components of the geometry are unchanged and therefore should be similar to those in the other cases.

From figure 10 it can be seen that there is not a boundary layer on the floor of the domain. This is due to the physical phenomenon of the car moving through the air rather than the method used in the experimentation, and simulation, of moving the fluid over the car. This

therefore has been implemented with a moving floor boundary at freestream velocity to eliminate the boundary layer on the floor.

From figure 10 it can also be seen that there is a cavity on the underside of the geometry. This, with the presence of the shear layer generated can become a resonating cavity. This can be seen by the velocity fluctuations in the cavity. This resonating velocity field can cause difficulties in capturing the coefficient of pressure, which is why there is a noisy coefficient of pressure plot for case 3. This cavity is not present on case 1 or 2 and therefore the result is a lot less noisy.

From figure 11 it can be seen that there are vortices produced developed at the rear of the car, similar to those produced with the Ahmed body. This does imply that the Ahmed body does have some automotive relevance. It can also be seen that the flow simulated is not unphysical and does show what is expected of flow over such geometry.

There are also vortices developed from the car bonnet down the side of the car. These vortices have altered paths in case 3 as the wing mirrors cause the vortex to be moved upward following the line of the window pillar.

It can also be seen that the rotation of the wheels cause a large amount of fluid to be forced forward. This, then, is transported downstream by the flow over the geometry. This can be seen by the large region by the door of the geometry.

6.5. OpenFOAM discussion

From the coefficient of pressure plots it can be seen that OpenFOAM is accurately predicting the flow. However how this relates to a discrepancy in the force calculations is unclear. It would be logical that as the coefficient of pressure plots agree with the experimental so would the drag coefficient as with the other solvers. This led onto there possibly being some error with the force calculation. This was investigated along with an investigation as to why the third case was unable to run.

It was believed that there may be a possible implementation issue as in the third case the simulation diverged and large errors were introduced. It is unclear as to why the case did this as the same input files were used for all of the cases, and the coefficient of pressure profiles for the first two cases are in good agreement with experimental data.

Initially it was suspected that the reason why the third case would not run was due to input file error. This was checked against the experimental data and the input files were discovered to give the correct initial conditions and boundary conditions. This, along with the first two cases providing great agreement with the coefficient of pressure plots, rules out there being an error in the input files.

This led to the implementation of the equations being checked against that of the publications for the models. This involved checking the implementation term by term against the publications of the models. Unfortunately no discrepancies were observed. It is currently unclear as to why the third case failed when two of the other solvers were able to run, and get accurate results, from the same meshes which rules out the mesh being the issue.

As to why the coefficient of pressure plots are in agreement with experimental and the forces are not led onto the suspicion that there are some errors with the force calculations. These were investigated. These investigations are still ongoing.

6.6. Methodology discussion

As the project progressed there was an increase in efficiency in CAD clean-up. This was due to the software being used becoming familiar and using the programs short cut features in order to decrease time taken. Further to this there was a decrease in time taken as more efficient processes were used for CAD clean-up throughout the project as a deeper understanding of what is required for CAD clean-up was achieved.

As the geometry was modular each module was cleaned once and then imported in to generate the cases. This helped reduce time as the main body geometry required cleaning once rather than for each individual case.

Following similar reasoning to that of the CAD clean-up the process efficiency for meshing increased as the project developed. The main decrease in time was that regions of high geometry gradient and detail could be specified to generate small cells automatically. This reduced the overall time taken as each of these regions did not require much manual alterations. This also helped reduce the overall skewness and orthogonality which led to a reduced manual time iterating the quality of the meshes so that they conformed to the criteria outlined previously.

For the solver, once the input file had been specified and that the file had been compared to ensure accuracy between it and the wind tunnel experiment, there could be little increase in solver process efficiency. As this was a totally automated process there was no room for improvements in the process efficiency.

The post process was again similar to that of the solver. Once the python script had been written then the post processing could occur automatically. Therefore as long as the script was calculating what was being compared there was little chance of this becoming more efficient.

Both the solving and post processing phases of the project were entirely automated and there has been little chance of increasing efficiency in these regions. CAD clean-up and meshing being time consuming for the user had the efficiency increased for each of the processes.

Further to this it is difficult to quantify the error associated with results from a simulation. The reason for this is that it is difficult to quantify the systematic or random errors introduced which could impact the results.

6.7. Significance of work

Significance of this work could cover a range of areas, including code validation, introducing industrially relevant test cases to industry, amongst others.

One significance of the work conducted would be code validation. Code validation plays a major part in whether the code agrees well with experimental data. Validation also shows the

capability of the solver and its aptness for use with specific engineering flows. For example there are some codes which are unable to solve more than the basic fluid flow equations and therefore would not be used for flows with chemical reactions. Therefore validation would be used by companies in their decision making as to which solver licence to acquire or indeed use open source software.

One other possible significance of this investigation would be that the test cases for automotive industry could be advanced. Conducting investigations into this case could help drive the industry to generate a collaborative test case where the geometry is of relevance to all areas of the automotive industry. This investigation could help generate collaborations between industries for the benefit of CFD automotive test cases.

The use of such an industrially relevant test case would hopefully bring the automotive industry to a similar stand point as the aerospace industry. Aerospace has the benefit of many industrially relevant test cases where the automotive industry does not. Hopefully one outcome from this project will be to help decrease the gap between automotive and aerospace validation.

By investigating an industrially relevant case with numerical methods derived primarily for aerospace may result in the development of numerical methods developed specifically for automotive industry. This could lead to a smoothing of the numerical methods from both the automotive and aerospace into one joint numerical method capable of solving both types of flow. However this does not seem to be required as the results agree strongly with the experimental data.

Another significance of this investigation could be the development of new modelling practices for the automotive industry. One example being how to model the grazing angle that the tyre makes with the road and which method, the contact patch method or the blocking method, would yield most accurate. This could be proposed to the industry or automotive community to help develop common modelling practice for these cases.

6.8. Conclusion

Results from the simulations for all three cases were accurate. Case 1 zCFD and Fluent matched the drag coefficient exactly at 0.115, OpenFOAM however had 50% error. For the second case, whose drag coefficient is 0.233, zCFD has 0.77% error, Fluent has 3% error and OpenFOAM has 19% error. For the third case, whose drag coefficient is 0.278, zCFD has 0.51% error and Fluent has 1.8%, OpenFOAM was unable to run. The error introduced was believed to be introduced when the wheel geometry was altered, by adding in a contact patch, to allow meshing.

There were some discrepancies with the coefficient of pressure plots, which may be attributed to unsteady flow being simulated in a steady manner. This was due to time constraints on this project being unable to solve an unsteady simulation as there is an associated increase of solution time. In general, however, the coefficient of pressure plots do agree well with the experimental data.

It was believed prior to the investigation, that the increase of detail would introduce modelling errors due to the discretisation during mesh generation being dissimilar to that of

the experimental geometry. This has been seen as errors are present but are assumed to be modelling decisions made with the wheel geometry by introducing a contact patch and not solely due to the increased detail.

From these results it was initially proposed that specific automotive models and numerical methods may need to be introduced. This is clearly not the case as the results agree very well with those given in the experiment. It is clear that even though there have been few automotive test cases due to the automotive industry adopting CFD at a later stage than aerospace has not had an impact on the accuracy of the solvers for automotive flow, and that techniques developed for aerospace are transferrable to the automotive industry.

As to the reasons why OpenFOAM captured the coefficient of pressure plots accurately but not the drag coefficient are still being investigated. These may be investigated with the OpenFOAM developers.

From the final flow regime it can be seen that predictions about the overall flow have been shown with the velocity profile, which supports conclusions drawn from the coefficient of pressure plots. Also shown is that the geometry chosen does indeed show the vortices produced by the rear geometry, which are similar to those present in the Ahmed body geometry.

6.9. Future work

The Centre for Modelling and Simulation (CFMS) located in Bristol has supported this project. As such CFMS has allowed access to its High Performance Computer (HPC) cluster for all simulation work required for this project. With nearly 3,500 cores of compute CFMS's cluster is capable of decreasing the time of simulations as CFD simulations can be run in parallel. Zenotech also have been very supportive on this project sharing its knowledge of CFD and best modelling practice along with giving access to its CFD solver.

Along with this support CFMS has organised events, one being on the 10th May 2016, for the results from this experiment to be presented to industry. There have been many sign ups to the event, one being McLaren. These presentations will be held at the offices of CFMS in Bristol and if accepted the final results being presented, and also published in the conference paper, at the International Conference on Vehicular Aerodynamics (ICVA) in September 2016 in Coventry.

Future work that will be further investigated for presentation at the conference will include the investigation of other turbulence models and their impact on the flow solution. Also following on from this, zCFD has recently implemented a high-order solver. This could be investigated and compared against the open source PyFR high order solver.

This high order methodology will be the main focus, as will the different turbulence models along with the continued investigation into what is causing the discrepancies with OpenFOAM.

7. Project management, consideration of sustainability and health and safety

7.1. Risk

Risk is a major part in all projects that are undertaken. Therefore it is important to determine and prevent risks in order for the project to run smoothly. Risk is considered anything that could have an impact on the project.

One risk would be that the geometry was given in an incompatible file format. This was alleviated by the use of a CAD package that can read in a variety of formats. With this the incompatible geometry, if applicable, would be read into an appropriate CAD software and exported to a format that would be applicable for the CAD clean-up software. Also the geometry was provided in two formats to alleviate this issue.

One possible risk to the project is that the CAD clean-up would take longer than expected. A method to alleviate this was to ensure that when the CAD was imported that the tolerance was set to cause some of the smaller gaps to be closed. Another method was that the CAD could be read into other CAD software which may join some of the gaps on import. All of these methods were used as some performed better for certain geometries. For example the detailed underbody required straight import rather than going through another software, due the number of small surfaces.

Another possible risk is that the meshing would take longer than estimated. This risk would be prevented by ensuring that the CAD was cleaned as best as possible. This ensured that when the CAD read into the mesh generator there would be minimum work required before meshing could start. An example of this is that during the CAD clean-up process there were some surfaces that intersected. These were trimmed as they could have caused issues during the meshing stage, which would then have taken longer, delaying the process.

One other possible risk is that the mesh generator would not be able to export the correct file formats for the meshes. To alleviate this risk OpenFOAM can support many user written applications. As such the converters, if not already written, could be written into OpenFOAM. This will not be as efficient as a direct export from the mesh generator. There would be a possibility that some of the accuracy is lost as multiple exports and conversions could introduce error, however accuracy and quality of the meshes was investigated prior to solution, if errors were introduced these would have been found prior to solution.

One risk is that the solution would take a long time, and would not be completed before the deadline. Hopefully the risk prevention mentioned previously would help in leaving ample time for the solution to be calculated and to converge. In order to prevent this risk the simulations would be run across many cores in order to speed up simulation time. This was not anticipated to be an issue as the cluster used had ample number of cores.

One other risk is that the solutions do not converge. This could be due to a number of issues. The major risk is that the mesh would be of incorrect quality. This was prevented by ensuring that all mesh quality statistics were at or below the maximum specified. One other could be

related to the input files or boundary conditions. This would be prevented by reading documentation and literature on how to correctly set up CFD cases.

One other possible risk is that the post processing takes an increased amount of time and results would not be able to be drawn before the deadline. One way to prevent this was to write a python script that calculated all parameters required for each case. This would then mean that the cases can be post processed in parallel, this would also mean that time was available to complete other tasks while the post processing was undertaken by the script.

7.2. Carbon footprint

Carbon footprint in computational engineering can be seen as two separate areas as it is difficult to fully quantify the carbon footprint of a simulation. One being solver and process efficiency and the other being accuracy of the solvers.

Solver and process efficiency

Solver and process efficiency relates to the time taken for the solution to be generated. With an increased process and solver efficiency reduces compute time used. As there are associated carbon footprints associated with electricity, using less would lead to a lower carbon footprint for the solution.

One other consideration is how much of the available hardware the software is able to use. If, for example, the solver utilises only 80% of the hardware, then this will take an increased time, and electricity, to one that is capable of utilising 95% of the hardware. Thus an efficient solver in terms of hardware utilisation is key to reducing the carbon footprint of the solution.

Solver accuracy

Increasing the accuracy of the solver and processes is key to generating reliable results. As accuracy increases there would be less reliance on expensive wind tunnel tests for each design. Wind tunnels are notoriously expensive and have a large carbon footprint to operate. Increasing accuracy of the solvers would lessen the use of these resulting in a lower overall carbon footprint.

Achieving a fast, efficient and accurate solver will have an impact on the number of designs investigated. This could potentially lead to an increased efficiency in the final product. This increased efficiency, in this case drag, would lead to less fossil fuels being used, which will lead to a decrease in the carbon footprint of the final product.

It can be seen that there is a carbon footprint associated with the solver and process and also the final design of products. It is not a direct relation to the CFD solvers but more of a by-product that increasing accuracy and efficiency of the CFD solvers relates to a lower carbon footprint.

7.3. Health and safety

There are few health and safety considerations required for this computational task. One major consideration is to ensure that the computer workstation conforms to the required

health and safety and ergonomic guidelines. This ensures that the user will not develop RSI or any other injuries.

One health and safety consideration taken into account while visiting CFMS was that while within the HPC data centre personal protection equipment was suggested to be worn, such as ear defenders, as the HPC was loud. Also ensuring that wires and cables are kept tidy to avoid tripping hazards is a priority health and safety consideration while in a data centre.

One other important consideration in health and safety is that as a computer screen would be used it is a requirement that there would be occasional breaks taken from viewing the screen. This reduces the chance of there being damage to the user's eyesight.

In terms of prioritising health and safety risk, one of the major risks would be that RSI would develop. This is mainly due to the constant use of the computer throughout the course of the investigation. Following this the next major health and safety risk would be eyesight damage. This again would be due to the continued use of a computer throughout. This is not as high risk as the user would be able to look away from the screen with relative ease.

Following this the lowest health and safety consideration would be hearing related as there will be little to no visitation into CFMS's cluster. Therefore this risk would still be around if there were to be a visit to the cluster.

7.4. Sustainability

In order for sustainability the methods and software have to be long lasting. There is an issue in the CFD industry that methods, hardware and numerics are regularly changing and being updated. Therefore there should be regular code updates and even possibly new software written for the new changes.

This means that the codes produced do expire fairly quickly and will need updating. In order for CFD software to be as sustainable as possible it must be capable of being easily updated. This would mean that other components and new research can be added to it with relative ease. This would mean re-using the core of the software and swapping components and utilities out for newer ones.

Also in order to be fully sustainable the code base must be as re-usable as possible. This means that writing efficient CFD codes that could be used in other applications means that the code is sustainable and can be used by a multitude of different programs. This would also mean that any improvements to the code base that could be introduced by other software would be ready to be used in the CFD code without having to re-write whole sections. Further to this by having a re-usable code base there could be other methods implemented in meshing, for example, that would benefit CFD solvers.

7.5. Project management procedures

In order to keep the project on track, various project management techniques were used. For instance to ensure that the project completed on time a critical path analysis was conducted. Along with the critical path analysis there was a Gantt chart produced.

Critical path analysis

Having produced a critical path analysis of the project it was clear that there needed to be some processes completed before further ones could begin. This mainly involved the meshes needing to be completed before the solution could be generated.

This was fairly common as the solution to the simple case, case 1, was investigated prior to the others. This was due to there being a possibility of modelling error, i.e. the boundary conditions being incorrect or the mesh being of inadequate quality, which could impact the results. These were identified during the initial case and then the input files were used for the later cases.

Gantt chart

Gantt charts produced helped identify the project milestones and set out the project schedule. This method developed a schedule and an understanding of the main tasks for the project prior to the project beginning. It was also used to help develop realistic goals and achievements and to ensure that the project was feasible in the time frame.

However as this project was mainly research based, the research being how accurate solvers are at high detailed automotive geometries, there, undoubtedly, were reasons why the Gantt chart could not be strictly adhered to.

Major reasons why the Gantt chart would not be definite is that it was unknown prior to the project beginning that one of the solvers would contain some issues, along with how long the individual processes would take. There were rough estimates based on previous work as to how long each process would take. It has been continually updated to adapt to the project.

Task Name	Duration	Start	Finish	Predecessors
Mesh Check	**3 days**	**Mon 11/01/16**	**Wed 13/01/16**	
Case 1	2 days	Mon 11/01/16	Tue 12/01/16	
Case 2	2 days	Tue 12/01/16	Wed 13/01/16	
Simulation Case 1	**8 days**	**Tue 12/01/16**	**Fri 22/01/16**	**2**
Fluent	8 days			
zCFD	8 days			
OpenFoam	8 days			
Simulation Case 2	**10 days**	**Fri 22/01/16**	**Fri 05/02/16**	**3,4**
Fluent	10 days			
zCFD	10 days			
OpenFoam	10 days			
Mesh Generation and Checks	29 days	Fri 15/01/16	Wed 24/02/16	
Simulation Case 3	**18 days**	**Wed 24/02/16**	**Mon 21/03/16**	**12**
zCFD	12 days			
OpenFoam	12 days			
Fluent	18 days			
Finished Simulations	0 days	Tue 22/03/16	Tue 22/03/16	
Post Process	**45 days**	**Mon 25/01/16**	**Fri 25/03/16**	
Case 1	2 days	Mon 25/01/16	Tue 26/01/16	4
Case 2	2 days	Mon 08/02/16	Tue 09/02/16	8
Case 3	4 days	Tue 22/03/16	Fri 25/03/16	
Finished Post Processing	0 days	Fri 01/04/16	Fri 01/04/16	
Initial Draft	18 days	Tue 01/03/16	Thu 24/03/16	
Final Draft	22 days	Mon 28/03/16	Tue 26/04/16	18,23
Finished Report	0 days	Tue 26/04/16	Tue 26/04/16	

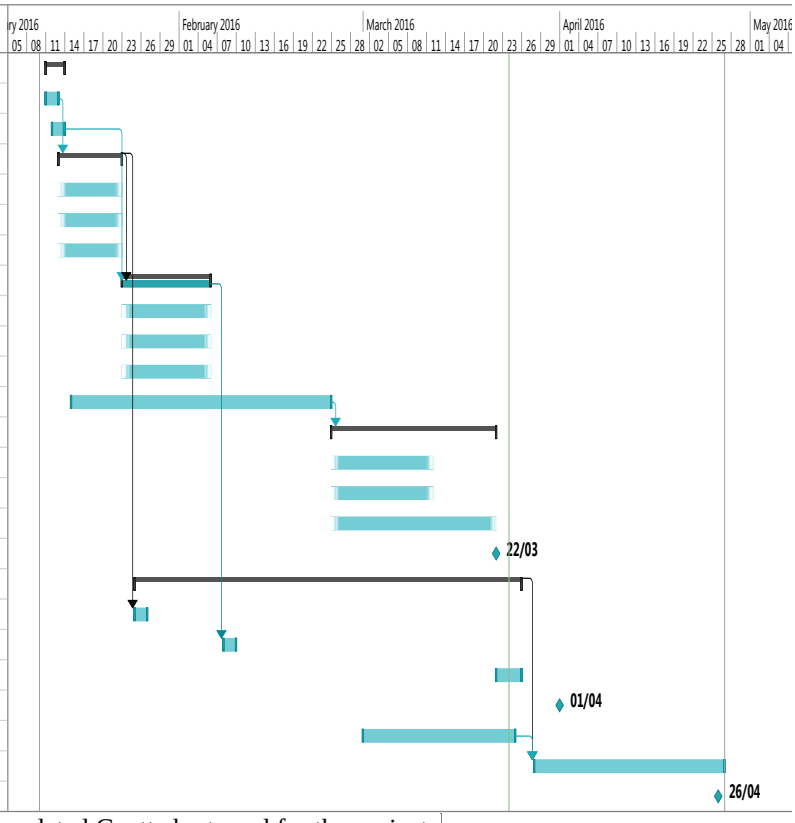

Figure 12: Showing the updated Gantt chart used for the project.

References

Ahmed, S.R., Ramm, G. (1984) Some Salient Features of the Time-Averaged Ground Vehicle Wake, SAE-Paper 840300

Ashton, N., West, A., Lardeau, S., Revell, A. (2016) Assessment of RANS and DES Methods for Realistic Automotive Models, Computers and Fluids 128 (2016) 1-15

Davidson, P.A. (2015) Turbulence: an Introduction for Scientists and Engineers. Oxford, Oxford University Press

Guilmineau, E. (2014) Numerical Simulations of Ground Simulation for a Realistic Generic Car Model, ASME 2014, August 3-7, 2014, Chicago, USA, FEDSM2014-21164

Heft, A., Indinger, T., Adams, N. (2011) Investigation of Unsteady Flow Structures in the Wake of a Realistic Generic Car Model, 29th AIAA Applied Aerodynamics Conference, June 27-30, 2011, Honolulu, Hawaii, USA, Paper AIAA 2011-3669

Heft, A., Indinger, T., Adams, N. (2012) Introduction of a New Realistic Generic Car Model for Aerodynamic Investigations, SAE 2012 World Congress, April 23-26, 2012, Detroit, Michigan, USA, Paper 2012-01-1068

Heft, A., Indinger, T., Adams, N. (2012) Experimental and Numerical Investigation of the DrivAer Model, ASME 2012, July 8-12, 2012, Puerto Rico, USA, FEDSM2012-72272

Jones, W.P., Launder, B.E. (1972) The Prediction of Laminarization with a Two-Equation Model of Turbulence, *Int. J. Heat Mass Transfer 15,* 301-314

Krajnovic, S., Davidson, L. (2004) Large eddy simulation of the flow around a simplified car model, SAE 2004 World Congress, SAE Paper 2004-01-0227, Detroit, Michigan, USA, 2004

Lee, D.T., Schachter, B.J. (1980) Two Algorithms for Constructing a Delaunay Triangulation, International Journal of Computer and Information Sciences, Vol. 9, No. 3, 1980

Lienhart, H., Becker, S. (2003) Flow and Turbulence Structure in the Wake of a Simplified Car Model, SAE 2003 World Congress, SAE Paper 2003-01-0656, Detroit, Michigan, USA, 2003

Lienhart, H., Stoots, C., Becker, S. (2000) Flow and Turbulence Structures in the Wake of a Simplified Car Model (Ahmed Model), DGLR Fach Symp. der AG STAB, Stuttgart University, 15-17 Nov., 2000

Menter, F. (1994) Two-Equation Eddy-Viscosity Turbulence Models for Engineering Applications. *AIAA J.* 32, 1598-1605

Minguez, M., Pasquetti, R., Serre, E. (2008) High-order large-eddy simulation of flow over the “Ahmed body” car model, Phys. Fluids, 20, 9, 2008

Owen, S.J., Staten, M.L., Cannan, S.A., Saigal, S. (1999) Q-Morph: An indirect Approach to Advancing Front Quad Meshing, International Journal of Numerical Methods in Engineering, **44**, 1317-1340 (1999)

Pope, S.B. (2015) Turbulent Flows, Cambridge, Cambridge University Press

Theissen, P., Wojciak, J., Heuler, K., Demuth, R. et al. (2011) Experimental Investigation of Unsteady Vehicle Aerodynamics under Time-Dependent Flow Conditions-Part 1. No. 2011-01-0177. SAE Technical Paper, 2011

Toro, E.F. (2009) Riemann Solvers and Numerical Methods for Fluid Dynamics, 3rd ed. Berlin, Springer

Versteeg, H. K., Malalasekera, W. (2007) An Introduction to Computational Fluid Dynamics The Finite Volume Method, 2nd ed. Essex, Pearson

Wilcox, D.C. (1988) Re-assessment of the Scale-Determining Equation for Advanced Turbulence Models, AIAA Journal, vol. 26, no. 11, pp. 1299-1310

Wojciak, J., Theissen, P., Heuler, K., Indinger, T. et al. (2011) Experimental Investigation of Unsteady Vehicle Aerodynamics under Time-Dependent Flow Conditions-Part 2. No. 2011-01-0164. SAE Technical Paper, 2011

Wordley, S.J., Pettigrew, J., and Saunders, J.W. (2007) Aerodynamics for Formula SAE: On-Track Performance Evaluation, SAE Paper 2007-01-0897, 2007

Wordley, S.J., and Saunders, J.W. (2006) Aerodynamics for Formula SAE: A Numerical, Wind Tunnel and On-Track Study, SAE Paper 2006-01-0808, 2006

Yazdani, R. (2015) Steady and Unsteady Numerical Analysis of the DrivAer Model, Master's thesis in Applied Mechanics, Chalmers University of Technology, Göteborg, Sweden 2015